Neutrons in coincidence with intermediate mass fragments at large angles from $^{14}N+Ag$ reactions at $E/A=20$ and 35 MeV

C. Bloch,* W. Benenson, A. I. Galonsky, E. Kashy, J. Heltsley,† L. Heilbronn, M. Lowe,‡ R. J. Radtke, and B. Remington§

National Superconducting Cyclotron Laboratory and Department of Physics and Astronomy, Michigan State University, East Lansing, Michigan 48824

J. Kasagi

Department of Physics, Tokyo Institute of Technology, O-Okayama, Meguro-Ku, Tokyo, Japan

D. J. Morrissey**

National Superconducting Cyclotron Laboratory and Department of Chemistry, Michigan State University, East Lansing, Michigan 48824

(Received 18 February 1988)

The spectral shape and multiplicity of neutrons from the reaction of $^{14}N+Ag$ at $E/A=20$ and 35 MeV have been measured for neutrons in coincidence with intermediate mass nuclei emitted at 50°, 70°, and 90°. The spectral shape clearly suggests two moving sources. The slower source velocity is about 80% of the center-of-mass velocity for $E/A=20$ MeV and 65% of the center-of-mass velocity for $E/A=35$ MeV (9% and 7% of the beam velocity, respectively). The faster source velocity is slightly less than half of the beam velocity for each case. Knowledge of the neutron multiplicity is necessary for models which attempt to explain the low effective temperature which has been determined from recent measurements of excited state populations. The data are also compared to the Boltzmann master equation approach of Harp, Miller, and Berne.

I. INTRODUCTION

The concept of nuclear temperature has been relatively successful in describing heavy ion reactions at both low ($E/A<10$ MeV) and high ($E/A>100$ MeV) bombarding energies.[1–6] The question has arisen as to whether the concept of temperature can be applied successfully to intermediate energy heavy ion collisions. In that case the temperatures are expected to be comparable to the separation energy of a nucleon in the nucleus. It is in this region that a liquid-gas phase transition has been postulated to take place.[7–9] Much of the experimental (e.g., Refs. 6, 8, and 10–19) and theoretical work (e.g., Refs. 9 and 20–26) in this energy region has focussed on thermodynamic concepts. Data in this energy range indicate that inclusive fragment yields depend on a power law[10] of the mass with the exponent in the range predicted by the thermal liquid drop model[27] for condensation around a critical point. In order to obtain a measurement of the temperature obtained in reactions in this energy range, we have investigated the reaction of $^{14}N+Ag$ at $E/A=20$ and 35 MeV.

Previous investigations of the above reaction at $E/A=20$, 25, and 35 MeV have reported measurements of the production of bound excited states of ^{7}Li and ^{7}Be nuclei emitted at large angles.[15,28,29] With certain assumptions, the distribution of emitted nuclei in their various excited states can be used to extract the temperature of the production source.[15] Specifically, if the nuclei are emitted from a thermalized source, their excited state populations should be given by a Boltzmann factor (ignoring spin factors). For a two level system in statistical equilibrium, the ration, R, of the population of the excited state to the population of the ground state is given by

$$R=\frac{2j_{ex}+1}{2j_{g.s.}+1}\exp(-\Delta E/kT)\ , \tag{1}$$

where $j_{g.s.}$ and j_{ex} are the spins of the ground and excited states, respectively, and ΔE is the energy difference between the states.[30] The temperatures extracted from the previously observed excited state populations were dramatically low (around 0.5 MeV). Another method of extracting a temperature from such reactions is via the moving source model,[11] which is fairly successful at describing the inclusive energy spectra of such fragments. In that model, a set of nucleons moving in the lab frame emits fragments with an energy dependence that is dominated by a factor of $\exp(-E/kT)$, where E is fragment energy in the rest frame and kT is an emission temperature. Fits to inclusive energy spectra using such a model indicate temperatures from 10 to 12 MeV for the reaction in question,[15,28,29] in sharp contrast to the temperature extracted from the excited state population measurements. In addition, recent measurements of unbound excited state populations in similar reactions, yielded temperatures around 3 to 5 MeV.[17,31,32] This again is significantly lower than the observed inclusive energy spectra slope parameters and significantly larger than the temperatures extracted from bound state populations of lower excitation energy.

Two frequently discussed mechanisms that might explain these apparent discrepancies are final state interactions[33] and sequential decay.[26] This work reports on measurements which bear on both explanations. Both of these possible explanations for the apparent discrepancies focus on the difficulty involved in directly measuring the original (i.e., at the time of thermal emission) population of low lying states (including the ground state). For experiments which measure relative populations of bound excited states, the accessible quantities are the population of the excited state, obtained by observing its associated γ ray, and the total fragment production in the ground and γ-emitting states, obtained with a silicon $\Delta E-E$ telescope. Dividing those two numbers gives the fraction, f, of fragments observed in the excited state. If final state interactions and sequential decay are ignored, then f is related to the temperature through the ratio, R, in the following ways:

$$f=\frac{R}{1+R} \quad \text{or} \quad R=\frac{f}{1-f} \ . \tag{2}$$

One possible difficulty which arises in this type of measurement is that the ground state and the bound excited states of a system are the lowest in excitation energies, and this makes them strongly susceptible to the effects of sequential decay (a process that in general preferentially feeds the lowest lying states).

For a given emission temperature, final state interactions can reduce the apparent temperature extracted from bound excited state measurements. An equilibrated system will emit fragments with an initial distribution of excited states described by Eq. (1). In the previous bound excited state population measurements, the populations were determined by observing the γ ray emitted in the deexcitation. If the excited fragment interacts with other particles, particularly neutrons, emitted from the same reaction, it can deexcite without emitting this γ ray. The mechanism just described is identified as "final state interactions." Boal made one attempt to calculate the effect of this process.[33] In addition to several theoretical assumptions, Boal was forced to estimate the associated neutron multiplicity since no data for this existed. The first goal of this experiment, was to measure these associated multiplicities.

The relevant neutron multiplicities are those associated with the fragments for which the bound excited state populations were previously measured. These fragments are intermediate mass fragments ($4<A<A_p$) observed at large angles (typically, $\theta_{\rm lab}\geq 50°$). The reason that those particular fragments were selected in those previous measurements is significant. The observation of intermediate mass fragments at large angles in the lab has been an important component of studies of reactions of this nature.[6,16,19,34–37] The importance of the large lab angle ($\theta \gg \theta_{\rm grazing}$) is to reduce the contribution from quasielastic processes.[6,37] This technique has been shown to be successful at biasing the data toward central, high multiplicity events.[6,34,36] Simple one step processes would not produce such large fragments at such large angles. There are many inclusive measurements of intermediate mass fragments.[10,11,13,16,36–39] Such spectra may contain particles from peripheral collisions and hence would not reflect the temperature of the complete projectile/target system and all of the available energy. Contributions from such processes are forward peaked, and in order to select central collisions, we have excluded the forward angles.

In addition to their relevance to final state interactions, coincident neutron multiplicities have other physical significance. Previously, there have been many experiments with neutron coincidences (e.g., Refs. 40–51). But in all previous experiments, the neutrons were measured in coincidence with one or more of the following: projectile-like fragments, fission fragments, or evaporation residues. The present measurement is unique in that it is the first time that neutrons have been measured in coincidence with intermediate-mass fragments at large angles. Considering the significance of these fragments in intermediate energy heavy ion collisions, these measurements could be an important key to understanding the mechanisms involved. This paper reports the associated neutron multiplicities for neutrons in coincidence with ^{6}Li, ^{7}Li, ^{8}Li, ^{7}Be, ^{9}Be, ^{10}Be, ^{10}B, and ^{11}B fragments observed at 50°, 70°, and 90° in the lab from the reaction of ^{14}N+Ag at both $E/A=20$ and 35 MeV. Furthermore, for fragments observed at 50°, the associated multiplicities are reported both for neutrons in and out of the plane of the observed fragment.

The neutrons in coincidence with the intermediate mass fragments were binned in kinetic energy spectra. These spectra were fit with a two-source moving source model.[11] Use of this model has several benefits. First, it provides an excellent parametrization of the data in terms of six parameters. Two of the parameters in this mode are the associated neutron multiplicities for the two apparent neutron sources. This facilitates the immediate extraction of one of the desired physical quantities, namely the associated neutron multiplicity. Second, this model provides an analytic expression for the neutron spectra (in the nonrelativistic limit), which is easily integrated over solid angle to give an expression for the neutron energy distribution, $(d\sigma/dE)$. Putting the moving source fit parameters into that expression produces a histogram of the energy distribution. This histogram can be then readily compared to predictions made by the Boltzmann master equation approach of Harp, Miller, and Berne as modified by Blann[20] (HMB model). A discussion of the physical implications of the other moving source parameters and the HMB model comparison is included.

II. EXPERIMENT

The experimental details are similar to those described in Ref. 50. Beams of 490 MeV $^{14}N^{5+}$ and 280 MeV $^{14}N^{4+}$ ions were provided by the K500 cyclotron of the National Superconducting Cyclotron Laboratory at Michigan State University. The target was a self-supporting foil of natural silver, 1.8 mg/cm^2 thick, with its normal at either 25° or 45° with respect to the beam. The beam passed through the target, and the current was measured in a shielded Faraday cup, roughly 10 ft from the target.

Charged particles were detected in four silicon $\Delta E-E$

telescopes each with a 300 mm^2 area. The silicon detectors were located inside the scattering chamber with polar angles (with respect to the beam direction), θ, of 50°, 70°, and −90° in a horizontal plane (azimuthal angle $\phi=0$), and the fourth detector was located at $\theta=50°$, $\phi=90°$ (below the beam axis in a vertical plane with the beam). The detectors were in aluminum mounts, which had provisions for liquid cooling. Refrigerated alcohol was run through channels in the mounts to keep the temperature at approximately −30 °C throughout the experiment. The two telescopes at 50° had ΔE detectors 100 μm thick, while the other two telescopes had ΔE detectors 50 μm thick. The E detector of each telescope was 1000 μm thick. The front of each telescope was covered with a gold foil 3 mg/cm^2 thick to reduce the number of heavy reaction products hitting the ΔE detector. Rare-earth magnets were fastened to the detector mounts above and below the ΔE detector to deflect electrons. Each of the four telescopes was placed approximately 17.6 cm from the target, and the solid angles of these detectors were determined by placing a 1.5 μCi ^{241}Am source in the target ladder. The ΔE elements of the telescopes were found to have solid angles of about 9.6 msr. For the data runs the E element of the telescopes limited the solid angle. These were approximately 0.7 cm behind the ΔE elements, which gives a telescope solid angle of 8.9 msr. With the use of these cooled detector telescopes, isotopically-resolved inclusive energy spectra were obtained for fragments which were identified as ^{6}Li, ^{7}Li, ^{8}Li, ^{7}Be, ^{9}Be, ^{10}Be, ^{10}B, and ^{11}B. Events with particles of charge 1 or 2 were electronically rejected on line by a Motorola 68 000 microprocessor.[52]

Neutrons were detected in coincidence with the fragments listed above in any of ten liquid scintillators. The scintillators were approximately 1 liter of NE213 in a sealed glass cell approximately 12.7 cm in diameter and 7.6 cm thick. These were located in the horizontal plane at angles of 20°, 50°, 70°, 120°, 160°, −30°, −70°, −90°, −110°, and −140° with respect to the beam. A schematic diagram of the detector positions is given in Fig. 1. The front of each of these detectors was located 125 cm from the target, with the exception of the 20° neutron detector, which was 200 cm from the target. The typical neutron detector had a geometric solid angle of approximately 7.5 msr. Immediately in front of each neutron detector was a 0.6 cm thick plastic paddle (NE102A) that was used to veto electronically events where charged particles struck the neutron detectors.

The in-beam background of scattered neutrons was measured by taking data with shadow bars between the neutron detectors and the target. The shadow bars were brass cylinders approximately 7.6 cm in diameter and 29.5 cm in length. These were positioned to overlap the solid angle subtended by the neutron detectors.

III. DATA ANALYSIS

The energy calibration of the silicon detectors was determined with calibrated pulsers. A check of the pulser calibration was made by comparing the energy range for a given isotope to what is expected based on the

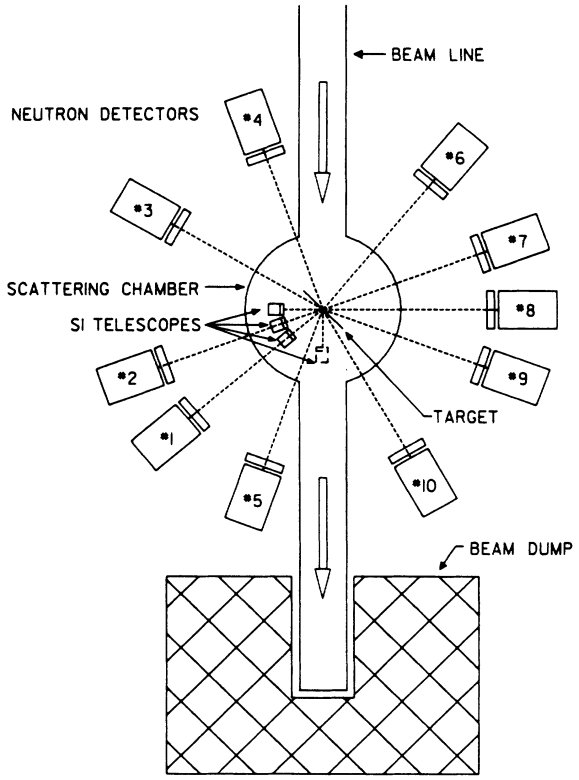

FIG. 1. Schematic of experimental setup.

detector thicknesses and the stopping ranges given in Ziegler.[53] In no case was any error discernable.

The neutron time-of-flight was measured relative to the charged particle signal from the front (ΔE) detectors of the silicon telescopes. Therefore, meaningful time information was only obtained for coincidence events. The time between the nuclear event and the silicon telescope signal was established from the target silicon detector distance, the particle mass, and the particle energy. The only coincident events considered were fragment-neutron coincidences.

The total range of time information for events in the neutron detectors in coincidence with telescope events, extends over nearly five cyclotron periods (for $E/A=20$ MeV) or about 340 ns. For neutron energies of 1 MeV or more, the true coincidences end before the end of two periods, so the first two cyclotron periods (from 0 to 138 ns for $E/A=20$ MeV and from 0 to 105 ns for $E/A=35$ MeV) were considered the real plus accidental coincidences. These events were corrected for indirect neutron events by the subtraction of a scaled (by the ratio of the integrated beam currents) version of the same histogram for data runs with shadow bars in place. The second two cyclotron periods (from 138 to 273 ns for $E/A=20$ MeV and from 105 to 209 ns for $E/A=35$ MeV) were considered to be the accidental coincidences, and subtracted from the real plus accidental coincidences (after both were corrected for indirect neutrons by subtraction of the appropriate shadow bar data) to yield the true real coincidences. This technique was used throughout the analysis, for each neutron histogram.

Considerable beam time (about $\frac{1}{3}$ of the total experiment) was devoted to the shadow bar runs so that their statistical uncertainty would contribute minimally to the final data. The net statistical uncertainty was obtained by taking the square root of the sum of the squares of the individual uncertainties.

The time to digital converters (TDC's) were calibrated by comparing the periodicity of the time-of-flight histogram to the period of the cyclotron. The time-of-flight histogram gated on γ rays (eliminating the neutron signals by pulse shape discrimination) for each neutron detector in coincidence with a signal from any particle telescope showed five γ-ray peaks for the $E/A=20$ MeV data and six for the $E/A=35$ MeV data. The average change in the pack centroid channel number was set equal to the cyclotron period to give the TDC calibration.

The neutron detector efficiency was determined for each neutron detector with the analytic code TOTEFF.[54] In Ref. 50, TOTEFF was compared to a Monte Carlo code developed by Cecil *et al.*[55] Based on that comparison, the uncertainty in the absolutely neutron detector efficiency is approximately 10%. The systematic errors in the present data are primarily due to uncertainties in determining the neutron detector efficiency ($\pm 10\%$). TOTEFF requires as input the detector threshold in electron equivalent energy. To obtain these thresholds, it was necessary to determine the calibration of the neutron detector pulse height.

The electron equivalent energy of the neutron detector pulse heights was calibrated using three different γ sources: ^{22}Na, ^{60}Co, and ^{212}Pb. The Compton edge for each of the observed γ rays was defined to be at half the maximum value of the step function. The γ rays observed were 0.511 MeV and 1.27 MeV from the ^{22}Na, 1.25 MeV (average of the 1.17 and 1.33 MeV γ rays) from ^{60}Co, and 2.62 MeV from the ^{212}Pb. From these energies, the maximum possible energy deposited via Compton scattering was calculated. A linear fit between these latter energies and the Compton edge channel number gave the calibration of the pulse height in electron equivalent energy. This information was used to determine the lower cutoff of the pulse height in electron equivalent energy, which was used as input to determine the neutron detector efficiency.

Charged particle inclusive data were taken with the neutron coincidence requirement removed from the master gate. Particle identification gates were set on the $\Delta E-E$ histogram for each telescope for each of the following isotopes: ^{6}Li, ^{7}Li, ^{8}Li, ^{7}Be, ^{9}Be, ^{10}Be, ^{10}B, and ^{11}B. The particle inclusive data were then binned into kinetic energy spectra for each isotope in each telescope. Typical spectra are shown for the $E/A=20$ MeV data in Fig. 2 and for the $E/A=35$ MeV data in Fig. 3. The solid lines shown in these two figures represent the moving source analysis described below.

For each isotope identified, the kinetic energy spectra were fit by a moving source model.[11] A single parameter set of normalization, slope parameter (kT in the temperature interpretation) and source velocity was obtained for all spectra of a given isotope. A Coulomb shift[56] was employed, where the shift was a fraction of the Coulomb barrier between the observed fragment and the residual nucleus. The fit parameters (including the Coulomb shifts used) are given in Table I for the $E/A=20$ MeV data and in Table II for the $E/A=35$ MeV data.

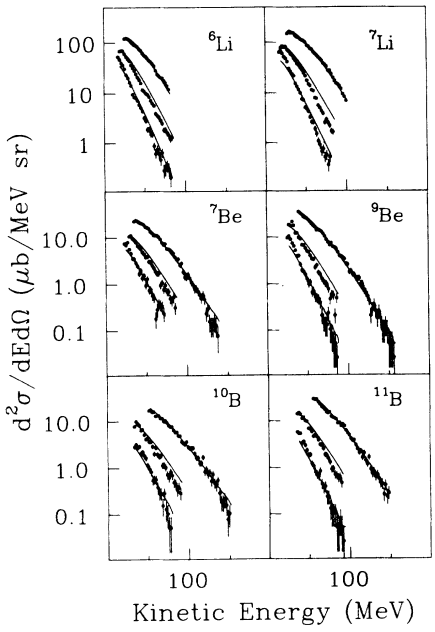

FIG. 2. Fragment kinetic energy singles spectra with moving source fit, $E/A=20$ MeV. Spectra are from detectors at 50°, 70°, and 90°.

Signals from the neutron detectors were due to either neutrons or γ rays (since charged particle events were identified by the thin plastic paddle in front of each neu-

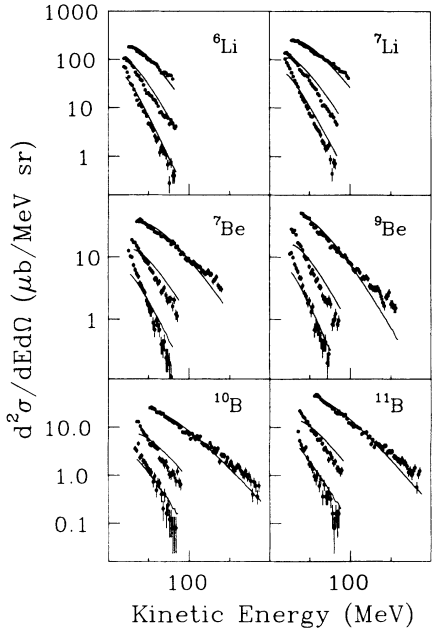

FIG. 3. Fragment kinetic energy singles spectra with moving source fit, $E/A=35$ MeV. Spectra are from detectors at 50°, 70°, and 90°.

TABLE I. Fragment kinetic energy moving source fit parameters for $E/A = 20$ MeV. The values in parentheses represent the uncertainty of the last significant figure.

Isotope	Coulomb shift (MeV)	σ (mb)	T (MeV)	β	χ^2/dof	#dof
^{6}Li	10	32.5(1)	10.3(3)	0.067(3)	20.6	92
^{7}Li	10	49.8(1)	11.3(4)	0.068(2)	42.5	99
^{8}Li	10	6.1(1)	13.3(5)	0.058(1)	6.8	99
^{7}Be	13	8.0(1)	11.5(3)	0.072(3)	4.0	103
^{9}Be	13	12.4(1)	10.8(4)	0.066(1)	6.3	113
^{10}Be	13	6.9(1)	11.6(7)	0.067(1)	3.6	108
^{10}B	16	9.2(1)	11.6(3)	0.071(3)	3.9	99
^{11}B	16	18.0(1)	11.0(4)	0.069(1)	3.5	110

tron detector and rejected electronically). Neutrons were distinguished from γ rays by pulse shape discrimination above a software threshold of approximately 200 keV electron equivalent energy, independent of the time of flight. The pulse shape discrimination was carried out with a 2-QDC (charge integrating ADC) method.[57] The signal from the anode of the neutron detector photomultiplier was split and fed into two QDC's. Each QDC began integrating at the same time, but one integrated the total charge, Q (over approximately 300 ns) while the other only integrated the charge collected in approximately the first 30 ns, ΔQ. In a plot of Q vs ΔQ, two distinct groups can be seen. One group corresponds to γ rays, which deposit a greater fraction of their total energy in a short time than do neutrons, the other group. Software gates were set on the neutron groups for each neutron detector with thresholds near 200 keV electron equivalent energy. The gain on the neutron detector signals was set high to get maximum resolution at low energies, when the two groups (neutrons and γ rays) in the $\Delta Q - Q$ map are close together. In order to retain the events that would otherwise end up in the overflow channel, attenuated versions of these signals were fed into a second pair of QDC's. The final neutron spectra are a combination of all events that could be identified as neutrons in either $\Delta Q - Q$ map.

The neutron kinetic energy was determined from the time of flight measurement, described above. The distance from the target to each neutron detector was measured, and when combined with the neutron time-of-flight, allowed calculation of the neutron kinetic energy on event-by-event basis. The neutron detector efficiency as a function of energy was calculated with the code TOTEFF[54] and folded into the neutron data. Figure 4 shows all 10 neutron spectra with the neutron detector efficiency included. Similar kinetic energy spectra were generated for neutrons in coincidence with each charged particle, in each telescope, and for each neutron detector. These spectra were then fit with a two-source moving source model.[11] The double differential multiplicity, $(d^2M_0/dE\,d\Omega)$, is given by (summation over index i from 1 to 2 implied)

$$\frac{d^2M_0}{dE\,d\Omega} = M_i \frac{\sqrt{E}}{2(\pi k T_i)^{3/2}} \exp(-E_s/kT_i) , \tag{3}$$

where

$$E_s = E - 2\sqrt{\epsilon_i E}\cos(\theta) + \epsilon_i , \tag{4}$$

and E is the neutron kinetic energy, θ is the neutron angle in the lab, M_i and kT_i are the associated neutron multiplicity and the slope parameter (temperature), respectively, for each source, and ϵ_i is the kinetic energy per nucleon of the source, given by

$$\epsilon_i = 931.5 \left[\frac{1}{(1-\beta_i^2)^{1/2}} - 1 \right] , \tag{5}$$

where β_i is the source velocity for each source in units of c, the speed of light. The prefactor of $\sqrt{E}$ in Eq. (3) arises for two different reasons for the two different sources. For the slower source, the temperature parameter indicates a relatively low excitation energy per nucleon. This implies "surface emission" of the neutrons, which for single neutron emission corresponds to a pre-

TABLE II. Fragment kinetic energy moving source fit parameters for $E/A = 35$ MeV. The values in parentheses represent the uncertainty of the last significant figure.

Isotope	Coulomb shift (MeV)	σ (mb)	T (MeV)	β	χ^2/dof	#dof
^{6}Li	10	54.8(1)	11.2(5)	0.075(2)	40.9	84
^{7}Li	10	92.4(2)	12.8(3)	0.081(1)	79.2	94
^{8}Li	10	12.9(1)	14.5(5)	0.070(4)	10.9	101
^{7}Be	13	18.0(1)	15.0(3)	0.098(3)	11.6	107
^{9}Be	13	20.5(1)	13.0(4)	0.083(2)	13.0	108
^{10}Be	13	13.2(1)	13.7(7)	0.082(1)	6.1	108
^{10}B	16	14.8(1)	15.0(4)	0.092(5)	6.8	119
^{11}B	16	28.1(1)	14.2(4)	0.086(4)	8.5	110

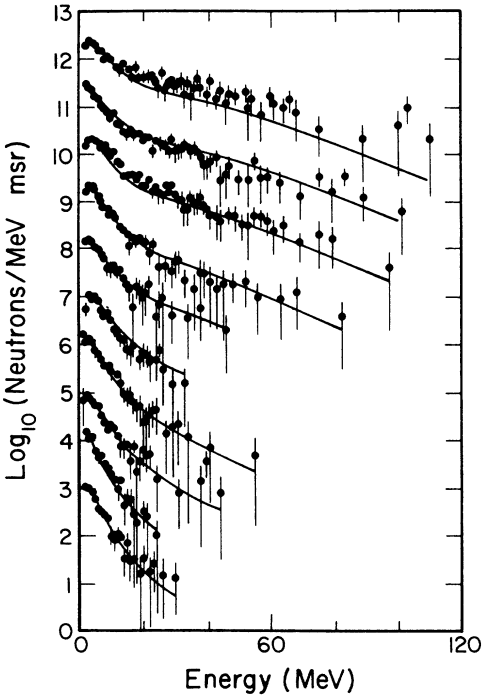

FIG. 4. Kinetic energy spectra for neutrons in coincidence with ^{7}Li at $\theta=50°$, $\phi=0°$ (data points) with two-source moving source fit (solid lines). The order of the neutron detectors (from top to bottom) is: 20°, −30°, 50°, −70°, 70°, −90°, −110°, 120°, −140°, and 160° in the lab. The spectra are separated artificially by an order of magnitude each, with the 160° data at unit normalization. $E/A=35$ MeV.

factor of E.[58] But the observed associated multiplicity indicates multiple neutron emission, which corresponds to a prefactor of $E^{5/11}$.[59] This has been approximated by $\sqrt{E}$. In this case, kT_1 is an effective temperature parameter. This is slightly less than the temperature of the daughter nucleus after the first neutron emission by a factor of $\frac{11}{12}$.[59] For the second source, the temperature parameters are much higher, and "volume emission" is assumed. In that case, the prefactor is $\sqrt{E}$.[58]

The neutron kinetic energy spectra fit parameters (M_i, kT_i, and β_i; $i=1$, 2) are shown in Table III for the $E/A=20$ MeV data and in Table IV for the $E/A=35$ MeV data. The parameters are listed separately for neutrons in coincidence with each isotope observed (^{6}Li, ^{7}Li, ^{8}Li, ^{7}Be, ^{9}Be, ^{10}Be, ^{10}B, and ^{11}B) and for each position of silicon detector ($\theta=50°$, 70°, and 90°, $\phi=0°$, and $\theta=50°$, $\phi=90°$). Generally, all 10 neutron detectors were included in each fit. The exceptions were for the $\theta=50°$ and 70°, $\phi=0°$ detectors when the coincident fragment was ^{6}Li, ^{7}Li, ^{9}Be, ^{10}Be, or ^{11}B. In those cases, the neutron detector that was colinear with the fragment detector was excluded from the fitted data. These cases were particularly sensitive to neutrons from the sequential decay of intermediate mass fragments in particle unbound states.[31,60] The coincident charged particle would be the residue from such a decay. For example, in Fig. 5 (neutrons in coincidence with ^{11}B at $\theta=50°$, $\phi=0°$, from the $E/A=35$ MeV data) the prominent peak near 7 MeV in the 50° spectrum is due to neutrons from the decay of the 3.388 MeV excited state of ^{12}B. The solid lines shown in Figs. 4 and 5 represent the double-differential multiplicity

TABLE III. Associated neutron kinetic energy moving source fit parameters for $E/A=20$ MeV. The values in parentheses represent the uncertainty of the last significant figure.

		Source #1			Source #2				
IMF	Angle	M_1	T_1	β_1	M_2	T_2	β_2	χ^2/dof	#dof
^{6}Li	50°	5.23(7)	2.54(6)	0.017(2)	0.91(5)	8.2(7)	0.089(6)	1.205	149
^{6}Li	70°	5.13(10)	2.44(8)	0.017(2)	1.38(10)	9.4(10)	0.05(4)	1.167	114
^{6}Li	90°	4.71(17)	2.1(9)	0.02(1)	1.83(17)	9.1(10)	0.034(18)	0.869	89
^{6}Li	50° [a]	4.71(7)	2.25(7)	0.015(1)	0.73(6)	11.1(10)	0.052(18)	1.196	131
^{7}Li	50°	5.07(5)	2.56(4)	0.019(1)	0.91(4)	11.8(8)	0.065(10)	1.573	176
^{7}Li	70°	4.75(9)	2.24(7)	0.019(10)	1.48(8)	8.5(10)	0.051(7)	1.556	125
^{7}Li	90°	4.91(12)	2.48(11)	0.021(2)	1.34(13)	11.0(10)	0.03(7)	0.818	107
^{7}Li	50° [a]	4.28(6)	2.36(3)	0.010(1)	0.57(3)	6.3(10)	0.08(4)	1.292	144
^{8}Li	50°	5.03(14)	2.51(12)	0.018(3)	1.08(17)	10.3(10)	0.07(3)	0.823	82
^{8}Li	70°	5.4(3)	2.6(2)	0.025(3)	2.1(4)	10.0(10)	0.02(4)	0.739	51
^{8}Li	90°	5.8(4)	0.59(14)	0.027(3)	5.0(4)	4.5(8)	0.011(1)	0.559	31
^{8}Li	50° [a]	4.01(18)	2.14(15)	0.009(7)	1.5(2)	9.7(10)	0.08(4)	0.773	62
^{7}Be	50°	3.74(13)	2.92(17)	0.026(3)	0.41(17)	8.2(10)	0.000(3)	1.299	65
^{7}Be	70°	3.8(3)	2.0(3)	0.018(5)	2.6(5)	9.8(10)	0.1(9)	0.894	37
^{7}Be	90°	5.2(7)	4.4(8)	0.02(2)	0.20(93)	9.5(10)	0.0(9)	0.379	8
^{7}Be	50° [a]	2.82(16)	2.8(3)	0.010(8)	0.01(26)	9.5(10)	0.00(3)	0.743	32
^{9}Be	50°	4.09(15)	2.08(13)	0.022(3)	2.40(15)	7.2(10)	0.028(25)	0.993	87
^{9}Be	70°	5.3(3)	2.20(19)	0.022(3)	3.4(5)	11.1(10)	0.03(6)	0.772	54
^{9}Be	90°	5.8(5)	2.4(6)	0.02(5)	1.9(10)	9.3(10)	0.1(8)	0.509	26
^{9}Be	50° [a]	3.31(14)	2.24(18)	0.020(3)	1.15(15)	6.1(10)	0.000(1)	0.775	64

TABLE III. (*Continued*).

IMF	Angle	Source #1 M_1	Source #1 T_1	Source #1 β_1	Source #2 M_2	Source #2 T_2	Source #2 β_2	χ^2/dof	#dof
^{10}Be	50°	4.84(19)	2.6(2)	0.021(4)	1.5(2)	11.3(10)	0.000(1)	0.819	60
^{10}Be	70°	5.4(4)	1.9(3)	0.024(4)	3.6(7)	11(2)	0.01(5)	0.663	35
^{10}Be	90°	6.4(9)	3.5(8)	0.02(10)	1.1(10)	9.5(10)	0.06(73)	0.229	10
^{10}Be	50° [a]	4.1(2)	2.5(3)	0.01(2)	0.8(9)	10.0(10)	0.10(17)	0.492	41
^{10}B	50°	4.28(17)	2.8(2)	0.017(5)	1.2(3)	10.0(10)	0.14(9)	0.793	60
^{10}B	70°	5.7(5)	1.4(2)	0.013(8)	6.8(8)	9.7(9)	0.061(57)	0.402	33
^{10}B	90°	9.6(7)	2.5(7)	0.008(8)	1.7(9)	5.0(10)	0.1(9)	0.627	5
^{10}B	50° [a]	4.7(2)	2.5(3)	0.012(6)	0.6(4)	9.8(10)	0.09(6)	0.548	42
^{11}B	50°	5.29(14)	2.71(13)	0.016(7)	0.97(19)	10.8(10)	0.12(8)	1.054	79
^{11}B	70°	6.5(3)	2.8(2)	0.016(7)	0.8(5)	1.7(6)	0.20(3)	0.667	47
^{11}B	90°	6.6(5)	1.8(7)	0.02(3)	5.0(10)	8.6(9)	0.13(11)	0.380	15
^{11}B	50° [a]	4.05(13)	2.5(5)	0.011(5)	1.0(3)	9.0(10)	0.15(5)	0.746	57

[a]50° out of the reaction plane.

TABLE IV. Associated neutron kinetic energy moving source fit parameters for $E/A = 35$ MeV. The values in parentheses represent the uncertainty of the last significant figure.

IMF	Angle	Source #1 M_1	Source #1 T_1	Source #1 β_1	Source #2 M_2	Source #2 T_2	Source #2 β_2	χ^2/dof	#dof
^{6}Li	50°	6.32(7)	3.07(5)	0.021(6)	2.02(6)	12.7(5)	0.096(4)	1.269	249
^{6}Li	70°	6.54(11)	2.98(5)	0.22(2)	2.00(10)	14.0(9)	0.101(8)	0.932	194
^{6}Li	90°	6.19(16)	3.23(17)	0.020(3)	1.97(18)	16.1(10)	0.143(17)	0.762	135
^{6}Li	50° [a]	6.05(7)	2.72(4)	0.016(1)	1.46(5)	11.0(5)	0.092(5)	1.142	224
^{7}Li	50°	6.48(6)	3.07(3)	0.020(3)	1.88(3)	12.5(3)	0.099(3)	1.689	291
^{7}Li	70°	6.35(10)	2.91(6)	0.019(1)	1.97(8)	13.7(7)	0.103(6)	1.036	218
^{7}Li	90°	6.33(14)	3.0(3)	0.020(1)	2.48(17)	19.4(10)	0.105(15)	0.814	162
^{7}Li	50° [a]	5.55(5)	2.81(4)	0.015(1)	1.19(3)	9.7(9)	0.116(13)	1.463	260
^{8}Li	50°	6.43(15)	2.80(10)	0.022(9)	2.56(13)	12.0(10)	0.084(16)	0.848	171
^{8}Li	70°	5.7(3)	2.9(2)	0.023(4)	2.8(3)	12.8(10)	0.042(38)	0.654	89
^{8}Li	90°	5.8(4)	2.3(3)	0.024(5)	5.0(6)	13.8(10)	0.020(36)	0.547	61
^{8}Li	50° [a]	5.09(15)	2.91(10)	0.015(3)	1.43(15)	12.2(9)	0.090(11)	0.810	107
^{7}Be	50°	7.23(13)	3.02(8)	0.022(2)	2.12(11)	11.9(8)	0.101(9)	1.172	181
^{7}Be	70°	6.9(3)	2.57(15)	0.023(9)	4.3(4)	15.8(16)	0.05(6)	0.696	103
^{7}Be	90°	7.5(6)	2.5(4)	0.01(2)	9.2(4)	23(9)	0.24(10)	0.474	38
^{7}Be	50° [a]	6.17(14)	2.60(9)	0.015(2)	1.56(13)	13.5(10)	0.088(18)	0.747	135
^{9}Be	50°	6.76(12)	2.79(9)	0.021(3)	2.29(12)	12.5(7)	0.096(7)	1.012	149
^{9}Be	70°	6.7(3)	2.54(18)	0.019(3)	3.9(3)	19.2(10)	0.09(4)	0.543	81
^{9}Be	90°	7.6(10)	2.2(10)	0.01(5)	2.6(8)	6.0(16)	0.13(9)	0.318	29
^{9}Be	50°	5.10(14)	2.81(12)	0.019(3)	1.47(14)	13.4(10)	0.101(17)	0.643	122
^{10}Be	50°	5.48(18)	2.88(16)	0.021(5)	2.7(2)	12.2(10)	0.076(12)	0.589	121
^{10}Be	70°	6.0(4)	2.0(4)	0.021(3)	4.6(5)	10.3(10)	0.07(3)	0.443	53
^{10}Be	90°	4.1(10)	3(7)	0.01(2)	6(9)	11(3)	0.1(7)	0.282	13
^{10}Be	50° [a]	5.30(18)	2.75(14)	0.011(9)	1.27(19)	11.3(10)	0.11(3)	0.708	85
^{10}B	50°	6.64(17)	2.79(11)	0.019(3)	2.5(2)	13.6(10)	0.077(14)	1.257	127
^{10}B	70°	6.4(3)	2.8(3)	0.028(5)	4.8(8)	14.6(10)	0.04(6)	0.483	54
^{10}B	90°	14.1(7)	3.4(5)	0.03(1)	4.5(10)	13.8(10)	0.128(11)	0.299	12
^{10}B	50° [a]	5.18(21)	2.38(8)	0.015(3)	2.4(2)	9.3(10)	0.053(16)	0.773	90
^{11}B	50°	7.06(14)	3.26(9)	0.025(4)	2.22(17)	21.0(17)	0.110(13)	1.081	151
^{11}B	70°	7.05(15)	2.82(2)	0.022(3)	4.0(5)	18.1(10)	0.02(4)	0.773	71
^{11}B	90°	9(14)	2(7)	0.02(5)	3.4(10)	10(4)	0.14(8)	0.492	15
^{11}B	50° [a]	5.14(15)	2.83(12)	0.015(4)	1.62(14)	10.4(10)	0.079(9)	0.833	121

[a]50° out of the reaction plane.

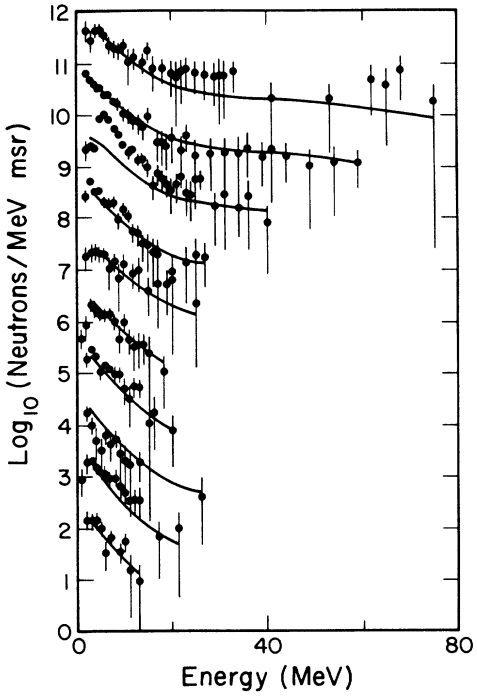

FIG. 5. Kinetic energy spectra for neutrons in coincidence with ^{11}B at $\theta=50°$, $\phi=0°$ (data points) with two-source moving source fit (solid lines), as in Fig. 4.

as calculated by Eq. (3) using the appropriate parameters from Table IV for each neutron detector angle. While such a calculation is shown for the colinear neutron detector, it should be remembered that the detector was excluded when determining the fit parameters.

The errors quoted for the fit parameters are the change in that parameter that corresponds to increasing χ^2 by 1, with all other parameters optimized. For each set of fit parameters, χ^2 per degree of freedom (χ^2/dof) and the number of degrees of freedom (#dof) is given. (The number of degrees of freedom equals the number of data points in the set minus the number of fit parameters, which in this case is six.) Caution should be exercised in interpreting the uncertainty of these fits. In some of the cases, the fit parameter errors are smaller than the maximum uncertainty of the fit parameters. This is because χ^2 is not a valid test for very small data sets.

IV. DISCUSSION

A. Intermediate mass fragments inclusive data

The kinetic energy spectra for each isotope identified were fit at all measured angles by a moving source model with a single parameter set (i.e., a single source), as described in the data analysis section. This is commonly done (e.g., Refs. 13, 16, 17, 35, 37, 39, 56, and 61–64), and it is done here for two reasons: (1) so these data would be easily comparable to other such measurements, and (2) because it provides a reasonable, convenient parametrization of the data. It should be stressed that this is only a parametrization, and the concept of a single moving source with a unique temperature is not to be taken literally. A more plausible description is that this source represents an ensemble average of sources with a continuum of velocities and temperatures.[6,37,65] Chitwood *et al.*[39] show three models with distinct physical differences that can fit this type of data equally well over this angular range. This illustrates that the moving source model's ability to fit the data is not necessarily proof of its physical significance. A more likely explanation for the ability of that model to fit the data is the limited angular range of the data.[36,37,39]

The moving source parameters extracted here are entirely consistent with previous measurements[15,28,29] and predictions based on similar reactions.[16,37,39] The fact that the moving source fit parameters are fairly independent of the isotope considered is one of the primary motivations for a thermal model.[11] However, any such model could have systematic errors which affect each observed slope identically and which would change a set of self-consistent temperatures into a different, yet still self-consistent, set of temperatures, as demonstrated in Ref. 39. For example, thermal modes generally ignore rotational energy. This energy is fluxed by angular momentum conservation, and should not be treated thermodynamically. Secondly, the treatment of the Coulomb shift is fairly critical. Each different way of estimating this quantity produces a different set of self-consistent temperatures. (The correction for Coulomb shift is, at best, an estimate. The magnitude is generally unknown, unless the target residue is detected. Even then, a two body process must be assumed.) While one method will usually produce the best fit (the lowest value for χ^2), there is some uncertainty in the significance of that result. The dependence of χ^2 on the Coulomb shift is most sensitive to the shape of the spectrum near the peak which is due to a combination of effects including the Coulomb barrier. However, the energy of the spectral peak is also usually quite near the lower threshold of typical silicon detectors, particularly for the heavier fragments. There is, naturally, always a question of whether the shape there is due to a change in the detector efficiency near its threshold. Since this is the energy at which there are the most counts, the statistical uncertainty is lowest here. This results in the highest weighting in determining the fit parameters, since systematic uncertainties are not generally included in the fitting routines. For these reasons, the kinetic energy slope parameter is best interpreted as being related to the temperature but not necessarily equal to it. (Certainly, for the same method of determining the fits and for the same detector, a higher slope parameter implies a higher temperature.) In these data, inclusive spectra exist at only 3 angles (50°, 70°, and 90°) over a limited angular range (40° in the lab). The fits to these data are not to determine the moving source parameters but to show consistency with fits to previous measurements. Finally, it should be noted that the fits to the ^{7}Li spectra (at both $E/A=20$ and 35 MeV) have the largest value for χ^2. This can be attributed in part to the contamination of these spectra by α pairs from the decay of

^{8}Be.[29] The spectra of α pairs has a different shape due to the geometric efficiency for detecting the coincident pair.

B. Coincident neutron data

The spectral shape of neutrons in coincidence with intermediate mass nuclei emitted at 50°, 70°, and 90° from the reaction of both $E/A=20$ and 35 MeV ^{14}N on Ag clearly suggests two moving sources. For the present data, a two-source moving source fit provides an excellent parametrization (χ^2 typically less than 1.3 per degree of freedom) in terms of the source velocities, the associated neutron multiplicities, and the slope parameters ("temperatures"). Unlike the charged particle data, no Coulomb shift is necessary in these fits. While two moving sources provide an accurate description, a third source leads to ambiguous results. This was demonstrated by Holub *et al.*[49] for very similar data with three-source fits. In the present work, the slower source has a velocity of about 80% of the center of mass velocity for $E/A=20$ MeV and 65% for $E/A=35$ MeV (or 9–7 % of the beam velocity), while the faster source has a velocity somewhat less than half the beam velocity for each energy (actually about 35% of the beam velocity).

1. Intermediate velocity source

For bombarding energies greater than 5 MeV above the Coulomb barrier, a process of neutron emission, typically described as nonequilibrium or preequilibrium (PE) neutron emission, is observed.[40,66] Preequilibrium neutron emission occurs in the early stages of formation and prior to the thermalization of the incomplete fusion system. While this process has been observed for some time, it is far from understood. Several distinctly different models have been suggested to explain this process,[24,67–70] each meeting with limited success. However, the moving source parametrization has been quite successful at describing the observed spectra. Typically, such a moving source has a velocity parameter from $\frac{1}{3}$ to $\frac{1}{2}$ of the beam velocity. This suggests that such emission occurs early in the collision process, specifically, after each projectile nucleon has undergone one or two nucleon-nucleon collisions.

The associated PE neutron multiplicities for the $E/A=35$ MeV data (given in Table IV) are consistent with predictions by Fields *et al.*[37] from associated proton PE multiplicities from a similar reaction (^{32}S+Ag at $E/A=22.5$ MeV). No left-right asymmetry [i.e., difference between the associated multiplicity for neutrons on the same side of the beam as the coincident intermediate mass fragments (IMF) and that for neutrons on the opposite side of the beam as the coincident IMF] is observed in the present data. This is consistent with what is observed for neutrons in coincidence with strongly damped projectile-like fragments in a similar reaction,[45,46,50] and in contrast to what is seen for neutrons in coincidence with quasi-elastic projectile-like fragments. This is further evidence that an IMF observed at a large angle is a good indication of a central collision. In addition, recoil effects[46] are not going to be pronounced since the coincident IMF is only a small fraction of the total mass and momentum and is not a strong trigger for the reaction plane or the target residue recoil.

Additionally, by comparing the multiplicities from the two detectors at $\theta=50°$ (one in the plane of the neutron detectors, $\phi=0°$, and the other at $\phi=90°$ with respect to the plane determined by the neutron detectors) the out-of-plane anisotropy can be determined:[40]

$$A_2=\frac{d\sigma}{d\Omega}(\phi=0°)/\frac{d\sigma}{d\Omega}(\phi=90°)-1\ . \tag{6}$$

For the $E/A=20$ MeV data $A_2=0.4\pm0.2$, while for the $E/A=35$ MeV data $A_2=0.5\pm0.2$ for the intermediate velocity source. This nonzero anisotropy indicates one of the limitations of the moving source model. The description of the neutron kinetic energy spectra given by Eq. (3) assumes isotropic emission in the rest frame of the emitter. The observed anisotropy indicates that there is actually a preferred plane of emission. Naturally, one would expect emission to occur preferentially in the plane normal to the angular momentum vector of the system. The observed anisotropy reflects not only the strength of that preference (which is determined in part by the magnitude of the angular momentum relative to the emission temperature) but also the degree to which the observed IMF determines the reaction plane.

Anisotropic emission implies a different polar angular distribution than that given in Eq. (3).[39,71–74] However, this difference is not obvious in the present spectra either for neutrons in the plane determined by the coincident IMF and the beam axis (shown in Figs. 4 and 5) or for neutrons emitted out of that plane (see Fig. 6). In order to fit the data in a consistent manner, an anisotropic

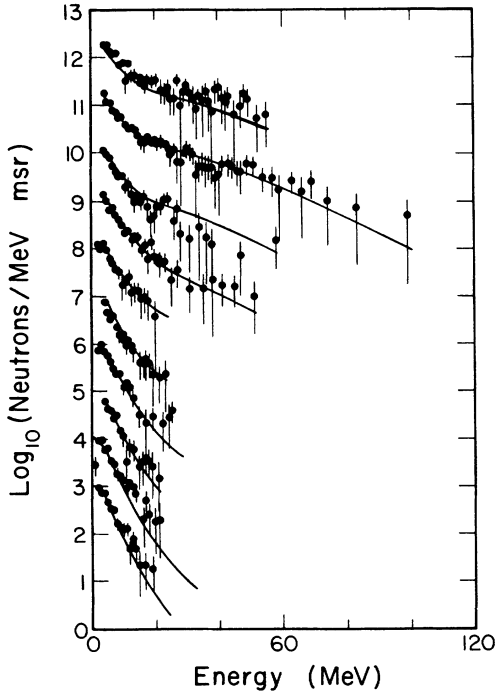

FIG. 6. Kinetic energy spectra for neutrons in coincidence with ^{7}Li at $\theta=50°$, $\phi=90°$ (data points) with two-source moving source fit (solid lines), as in Fig. 4.

model should be introduced. However, the present data would not provide a sensitive test of such a model. In part this is due to the fact that the observed neutron anisotropy is averaged over the azimuthal (with respect to the entrance channel scattering plane) IMF distribution. Rather than attempting to incorporate a complicated model which the data would not conclusively test, the anisotropy is included in the average multiplicity measurements in an empirical way. If the double differential multiplicity is expressed as

$$\frac{d^2M}{dE\,d\Omega}=[\cos^2(\alpha)+2\sin^2(\alpha)\cos^2(\phi)]\frac{d^2M_0}{dE\,d\Omega}\ , \quad (7)$$

where $(d^2M_0/dE\,d\Omega)$ is given by Eq. (3), then α is given by

$$\alpha=\arctan(\sqrt{A_2/2})\ . \quad (8)$$

This parametrization then describes the complete data set with the given parameters. In this representation, the in-plane ($\phi=0°$) multiplicities given in Tables III and IV are actually $[1+\sin^2(\alpha)]\times M$ while the out-of-plane ($\phi=90°$) multiplicities given in those tables equals $\cos^2(\alpha)\times M$. From these relations it is easy to see that the total multiplicity, M, is the linear average of the in-plane and out-of-plane multiplicities. The azimuthal parametrization given by Eq. (7) is actually similar to that conventionally used (e.g., Ref. 73), where the double differential cross section has a term of the form $\exp[-C\sin^2(\phi)]$. The similarity of these distributions (for appropriate normalizations) is shown in Fig. 7.

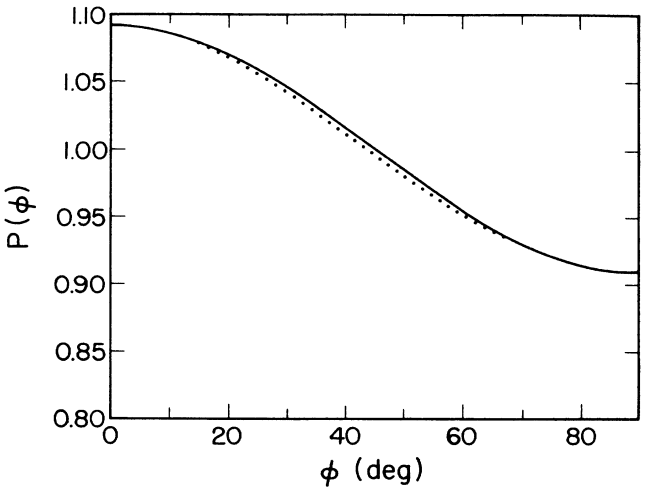

FIG. 7. Comparison of azimuthal (ϕ) distributions: $P_1(\phi)=\cos^2(\alpha)+2\sin^2(\alpha)\cos^2(\phi)$ (solid line) and $P_2(\phi)=N\exp[-C\sin^2(\phi)]$ (dotted line). Parameter alpha is chosen to describe the observed anisotropy. Parameters N and C are chosen to match the two functions of 0° and 90°.

2. *Final state interactions*

In the framework of these coincidence measurements, the importance of the PE neutron source is emphasized by the similarity between those fit parameters (given in Tables III and IV) and those for the intermediate mass charged particle inclusive spectra (given in Tables I and II). Considering the uncertainty in the parameters due to the Coulomb shift (for the IMF inclusive spectra), the parameters are sufficiently similar to suggest that they are parametrizations of the same moving source. (It is not possible to conclude, however, that the same physical process is responsible for the emission of both the neutrons and the intermediate mass charged particles.) Only the PE neutrons (not the sequential neutrons from the target like source) can interact with the observed intermediate mass fragments. Fragments emitted in bound excited states can be deexcited by interactions with other simultaneously emitted particles, which would lower the observed excited state population. This mechanism was previously put forth to explain the excited state populations reported in Refs. 15, 28, and 29. The neutrons from the target residue occur in a sequential process, and could not be available for final state interactions with intermediate mass fragments (the time of emission is too long).

In his paper on final state interactions,[33] Boal addresses the deexcitation of ^{7}Li from its first excited state ($E_{ex}=0.478$ MeV) via collisions with other nuclei being emitted from the same thermal system. The model assumes a single thermal source for the fragments and the neutrons, which can only be the PE neutron source. In comparing the observed temperature, T^*, to the actual temperature, T_0, Boal writes

$$\frac{T^*}{T_0}=\left[\frac{(\Delta\pi)^4\mu}{m(A\sigma)^2}\right]^{1/3}\ , \quad (9)$$

where Δ is related to the spatial extent of the expanding nucleon gas, μ is the ^{7}Li—n reduced mass, m is the nucleon mass, A is the equivalent number of neutrons in the gas (discussed below), and σ is the inelastic cross section for n+^{7}Li(0.478) for neutrons in the $\frac{1}{2}$–15 MeV region.

The parameter A is the number of neutrons that would produce the same probability for deexcitation as the actual mixture of coincident particles, if those particles were replaced entirely by neutrons. Boal assumes that this number A is between the number of coincident (complex) fragments and the number of coincident baryons (constituents of those fragments). For those limits, Boal used the values of 17.6 coincident light fragments and 28.4 coincident baryons, obtained from light particle multiplicities estimated as

$$M_p+M_n=12.7\ ,$$
$$M_d=1.4\ ,$$
$$M_t=1.1\ ,$$
$$M_\alpha=2.4\ .$$

Based on those limits, Boal chose a value of 20 for A in calculating the effect of final state interactions.[33] It now

appears that those values are all too large. Based on the neutron multiplicities reported in this paper and light charged particle multiplicities reported for a similar reaction,[37] a better estimate of the effective cross section is possible.

For $^{32}S+Ag$ at $E/A=22.5$ MeV, Fields *et al.* report an associated PE proton multiplicity of 2.0 for protons in coincidence with Li of momentum, $\langle P_x \rangle = 820$ MeV/c. (This momentum most closely resembles the typical momentum of ^{7}Li fragments observed in the $E/A=35$ MeV data presented here.) Based on the similarity between that measurement and the associated PE neutron multiplicity for neutrons in coincidence with ^{7}Li reported here for $E/A=35$ MeV (1.86 given in Table IV), the charged particle multiplicities reported in Ref. 37 are probably close to (or slightly larger than) the corresponding multiplicities for this reaction. Based on that, reasonable estimates for the $E/A=35$ MeV case are

$$M_p+M_n=4.0\ ,$$

$$M_d=0.5\ ,$$

$$M_t=0.3\ ,$$

$$M_\alpha=1.2\ .$$

Under this assumption, then, for $E/A=35$ MeV the number of coincident light fragments (including nucleons) is 6, and the total associated PE baryon multiplicity is 11. Therefore, $A=8$ is a better estimate than $A=20$ for this energy. Furthermore, at $E/A=20$ MeV the associated PE neutron multiplicity is approximately half the value at $E/A=35$ MeV. Under the assumption that all associated PE light fragment multiplicities have the same dependence on beam energy, the number of coincident light fragments is 3, and the total associated PE baryon multiplicity is 5 for the $E/A=20$ MeV case. Then for this case, $A=4$ is a reasonable estimate.

Putting numerical values into Eq. (9) gives

$$\frac{T^*}{T_0}=0.141\,A^{-2/9}\ . \tag{10}$$

For Boal's assumption of $A=20$, this gives $T^*=0.073T_0$. For $A=8$, as estimated here, $T^*=0.089T_0$, which is not significantly different from the result obtained by Boal. Finally, for the $E/A=20$ MeV case, $A=4$ yields $T^*=0.10T_0$, which is still not significantly different. While the present estimates of the associated charge particle multiplicities are probably somewhat too high (as indicated in the previous section), the overestimates are not significant in this context. In fact, if we have only one coincident ejectile (on average) then, $T^*=0.14T_0$. In order for final state interactions to be negligible, T^*/T_0 must be about 1, which occurs when $A=1.5\times10^{-4}$. This shows that Boal's model of cooling is very insensitive to the associated multiplicities. If the model is correct, significant cooling must always be present. Essentially, these associated multiplicities do not change the conclusions made in Ref. 33. However, as suggested in Ref. 28, Boal's model of the cooling represents a limiting case.

3. *Target-like source*

The mechanism responsible for the emission of neutrons from the slower source is certainly better understood than that for the faster source. For sufficiently low beam energies ($E/A<5$ MeV above the Coulomb barrier) the inclusive spectra can be parametrized by a single moving source.[40,75–79] At those energies, the projectile and target form a compound nucleus (for central collisions) which deexcites via neutron emission (among other processes). The formation of a compound nucleus creates special circumstances. First of all, no nucleons escape before the formation, so all of the beam's energy and momentum is transferred to the compound system. Secondly, the energy is sufficiently distributed among all of the nucleons in the system that statistical descriptions are applicable. To that extent, the system has thermalized or reached equilibrium.[5] The velocity obtained from moving source fits of the observed neutron spectra is the center of mass velocity. The slope parameter obtained from such fits will be related to the temperature of the compound nucleus residue after a single neutron emission by a factor of $\frac{12}{11}$.[59]

As beam energies are increased beyond 5 MeV/nucleon above the Coulomb barrier to the levels studied here, this process evolves into a slightly different process. The moving source fits to the neutron data indicate a source moving slower than the center of mass velocity for the compound system. This effect is related to incomplete fusion, which indicates incomplete momentum transfer from the beam. In the present data, for $E=280$ MeV, $\beta_1/\beta_{c.m.}=0.8$, while for $E=490$ MeV, $\beta_1/\beta_{c.m.}=0.65$ (i.e., 80% and 60% momentum transfer, respectively). (β_1 is the velocity obtained from the moving source fits for the target-like source, while $\beta_{c.m.}$ is the center of mass velocity, both in units of c.) The systematics of the data presented here indicate that this effect gradually becomes more pronounced for higher beam energies. This trend has been demonstrated before (e.g., Refs. 80–82), with plots of momentum transferred as a function of $\sqrt{(E-V_C)/A_p}$ (where E is beam energy, V_C is the Coulomb barrier transformed to the lab frame, and A_p is the number of projectile nucleons.) The present results lie well within the established trend.

A simple interpretation of the observed momentum transfer is that this indicates the average number of projectile nucleons that combine with the target in an incomplete fusion process to form the resulting compound system. The compound system that is formed is not unique; the number of nucleons involved will be a finite distribution about some average, which reflects the variations in impact parameters. Since some of the beam nucleons do not participate in the incomplete fusion, some of the momentum and energy from the beam will be "lost." In this interpretation, the velocity of the compound system is determined by the center of mass momentum as calculated for the fraction of the beam projectiles that participate. Similarly, the temperature of the compound system is determined by the energy available in the center of mass, excluding that carried off by other particles. This energy is given by[82]

$$E^* = \frac{\beta_1}{\beta_{\text{c.m.}}} E_{\text{c.m.}} + Q \ , \tag{11}$$

where β_1 and $\beta_{\text{c.m.}}$ are as previously defined, $E_{\text{c.m.}}$ is the incident lab energy transformed to the center of mass for the whole system, and Q is the Q value for the incomplete fusion reaction. Based on Eq. (11), the maximum excitation energies are 178 and 274 MeV for the 280 and 490 MeV beam energies, respectively (which includes Q values of -20 and -8 MeV, respectively, based on the reactions $^{14}\text{N}+\text{Ag}\rightarrow\text{Te}+2\text{p}+\text{n}$ and $^{14}\text{N}+\text{Ag}\rightarrow\text{Sb}+\text{p}+\alpha$). The corresponding temperatures based on the simple equation (which neglects rotational energy):

$$E^* = aT^2 \tag{12}$$

(where $a = A/8$ MeV^{-1} is the level density parameter, $A = 122$, and T the temperature), are 3.6 and 4.5 MeV, respectively. These upper limits are significantly larger than the experimentally observed temperatures of 2.7 and 3.3 MeV for the two energies (from $\frac{12}{11}$ times the slope parameter for the slower source). This difference can be reduced by considering an additional term in Eq. (11), the energy lost via cooling of the preequilibrium source.[51]

Fragment emission from the preequilibrium source reduces the available excitation energy for target-like source. Considering this energy, Eq. (11) becomes[51]

$$E^* = \frac{\beta_1}{\beta_{\text{c.m.}}} E_{\text{c.m.}} + Q - \langle KE \rangle_{\text{PE}} \ , \tag{13}$$

where $\langle KE \rangle_{\text{PE}}$ is the energy lost from all preequilibrium emission excluding that energy already taken into account by the $(\beta_1/\beta_{\text{c.m.}})$ factor in the first term in the above equation. Alternatively, one can estimate the portion of the missing momentum that is accounted for by preequilibrium emission, and replace the first term of Eq. (13) by $E_{\text{c.m.}}$ minus the energy corresponding to any *other* missing momentum. In that case $\langle KE \rangle_{\text{PE}}$ is simply all of the energy removed in preequilibrium emission. The latter approach is used here.

The extent to which preequilibrium emission accounts for incomplete momentum transfer depends on the *total* preequilibrium multiplicities. The moving source fits indicate that for the $E/A = 20$ MeV data, the total average missing momentum was equivalent to 3 nucleons at the beam velocity; for the $E/A = 35$ MeV case, 6 nucleons at the beam velocity can account for the missing momentum. As previously estimated, for $E/A = 20$ MeV, 6 preequilibrium nucleons are in coincidence with an emitted IMF (^{7}Li) for a total emission of 13 nucleons, while for the $E/A = 35$ MeV case that number is 18 (11+7). Based on those preequilibrium multiplicities and emission from a source with velocity approximately $\frac{1}{3}$ the beam velocity, preequilibrium emission accounts for all (or more) of the missing momentum. (The fact that the missing momentum attributable to preequilibrium emission exceeds the observed missing momentum, indicates that the estimates for the preequilibrium associated charged particle multiplicities are slightly high.) This indicates that no beam nucleons are missing, and the first term of Eq. (13) should be replaced by $E_{\text{c.m.}}$.

The simplest estimate of $\langle KE \rangle_{\text{PE}}$ then, is given by

$$\langle KE \rangle_{\text{PE}} = \langle M_f \rangle (\tfrac{3}{2}) T + (\tfrac{1}{2}) \langle M_{\text{N}} \rangle m_0 (\beta_2)^2 \ , \tag{14}$$

where $\langle M_f \rangle$ is the total average preequilibrium fragment multiplicity, $\langle M_{\text{N}} \rangle$ is the total average preequilibrium nucleon multiplicity, m_0 is the nucleon mass in MeV, and β_2 is the velocity of the preequilibrium source in units of c. (Here, "total" refers to the fact that these multiplicities include the IMF, in contrast with coincident multiplicities which indicate values in addition to the IMF.) Based on the previous estimates (for a ^{7}Li coincident IMF), for the $E/A = 20$ MeV case $\langle M_f \rangle = 4$ and $\langle M_{\text{N}} \rangle = 12$ while for the $E/A = 35$ MeV case $\langle M_f \rangle = 7$ and $\langle M_{\text{N}} \rangle = 18$. Typical values for T are 10 and 12 MeV for the two cases, respectively (as reported in Tables III and IV). This yields values of 73 and 161 MeV for $\langle KE \rangle_{\text{PE}}$, respectively. The Q value for the target-like residue was calculated for the target plus projectile minus preequilibrium fragments. The values obtained for Q were -34 and -57 for the $E/A = 20$ and 35 MeV reactions, respectively. Based on these values and Eq. (13), E^* (for the target-like residue) is 141 and 216 MeV for the two beam energies. Temperatures extracted via Eq. (12) with these values are 3.2 and 4.1 MeV. While somewhat higher than the values based on the slope parameter obtained from the neutron spectra (3.0 and 3.3 MeV, respectively), the agreement shows consistency within the level of approximation involved. (The value used for a was simply $A/8$ MeV^{-1}, where A, to be consistent with the target-like residue, was 110 and 104 for the two cases.)

The associated neutron multiplicities observed for the target-like source are consistent with those observed by Remington *et al.*[50] who measured the multiplicities for neutrons in coincidence with intermediate mass fragments (IMF's) observed at forward angles (7°–30° in the lab) from the reaction of $^{14}\text{N}+{}^{165}\text{Ho}$ at $E/A = 35$ MeV. Specifically, the "target-like source" multiplicities for "low energy light fragments (LE LF)" from that work should be considered. The selection of low energy fragments as a trigger excludes the quasielastic events which are not seen in the data presented here. The Remington data clearly exhibit an increase in multiplicity with increasing fragment lab angle. A linear extrapolation to 50° would result in associated multiplicities of 10 or more, slightly higher than those reported here (typically 6–7) for reactions at $E/A = 35$ MeV but on a smaller target nucleus. In contrast to the Remington data, the multiplicities reported here do not show a significant dependence on the lab angle of the coincident IMF. This is evidence that the dependence on IMF angle ends somewhere between 30° and 50° in the lab, where the maximum average multiplicity is reached. In that sense, an IMF at a large lab angle ($\theta \geq 50°$) is a good indication of a central collision. As for the PE neutrons, no left-right asymmetry is observed for the neutrons emitted from the target-like source.

Finally, for both $E/A = 20$ and 35 MeV data, the out-of-plane anisotropy, A_2, is 0.2 ± 0.1 for the target-like source. This anisotropy is less than that observed for the

intermediate velocity source. Qualitatively, this is predicted by the theory of Ericson and Strutinsky[71] which says that out-of-plane anisotropy should decrease with an increase in the moment of inertia of the source (for a given angular momentum). Again, no attempt was made to fit the data with an anisotropic model. While the statistics are better for this source, the anisotropy is less (and, hence, should have a reduced effect on the observed angular distributions), which again makes it difficult to observe a deviation from isotropy in the polar distributions.

4. *HMB model*

The Boltzmann master equation approach of Harp, Miller, and Berne as modified by Blann[20] for heavy-ion reactions, predicts the time evolution of the system with the Boltzmann master equation. The model considers the target plus projectile system in terms of single particle occupation probability densities for the total excitation energy available. For a given number of initial degrees of freedom, the model lets the system relax via either internal nucleon-nucleon scattering or particle emission over finite time steps ($\Delta t = 2.0 \times 10^{-23}$ s). The model can then predict the observed emission after any number of time steps. In the simplest model, the number of initial degrees of freedom, or exciton number n_0, is equal to the number of projectile nucleons, A_p.[20] Other descriptions have suggested that n_0 should equal $A_p + 3$, to approximate effects due to heavy ion collective degrees of freedom.[20,24,49] In addition, empirical results from some works have suggested an energy dependence for n_0.[42,49,64] The exciton number is primarily responsible for the shape of the energy distribution predicted by the HMB model.[20] The overall normalization is determined by the intranuclear transition rates, which are fixed parameters in the model.[20]

In addition to Z and A for both the target and projectile, the initial exciton number, and the beam energy, the HMB model requires the excitation energy as input. A brief discussion of the values used for the excitation energy is necessary. The excitation energy used here is not the value given by Eq. (13). That equation was used to predict the excitation energy of the targetlike evaporation residue, which excludes any energy lost from incomplete momentum transfer and preequilibrium processes. The HMB model does not preclude preequilibrium emission so that energy should not be excluded from the available excitation energy. There is, however, some error involved if all of the center of mass energy (plus the Q value) is used as the excitation energy in this model.

The problem arises because the HMB model (as used here) does not account for preequilibrium emission of heavy ions. This means that at some time in the reaction, the energy removed by the observed IMF becomes unavailable for neutron emission. This energy includes both a collective portion (A_{IMF} nucleons at the source velocity removed from the interaction) and the thermal emission energy ($\frac{3}{2}T$). In order to establish limits for this effect, the model was run both including any such energy, and with the energy excluded prior to the start of the reaction (i.e., removed from the initial excitation energy). Certainly the ideal method would be to include heavy ion emission in the model and let the energy become unavailable to other processes at the time of emission of the IMF. As yet, that is beyond the capabilities of this model.

As an upper limit, the excitation energy equals the center of mass energy plus the appropriate Q value. For $^{14}\mathrm{N} + {}^{107}\mathrm{Ag} \rightarrow {}^{121}\mathrm{Xe}$ the Q value is -3.1 MeV. For $^{14}\mathrm{N} + {}^{109}\mathrm{Ag} \rightarrow {}^{123}\mathrm{Xe}$ the Q value is -0.6 MeV. Since the target was natural silver (roughly a 50/50 mixture of the two isotopes) an average Q value of -2 MeV was used. This gave excitation energies of 246 and 432 MeV for the $E/A = 20$ and 35 MeV cases, respectively.

The lower limit for the excitation energy was calculated by estimating the energy removed by the observed IMF. If the IMF considered is ^{7}Li, for $E/A = 20$ MeV ($\beta_2 = 0.07$) the collective energy loss is 16 MeV, while for $E/A = 35$ MeV ($\beta_2 = 0.1$) that loss is 33 MeV. Subtraction of these values from the original lab energies, and transformation to the center of mass for $^{12}\mathrm{C} + {}^{103}\mathrm{Rh}$ (to account for the absence of the ^{7}Li nucleons) gives center of mass energies of 236 and 409 MeV for the two cases. Based on kinetic energy slope parameters of 10 and 12 MeV, the thermal energy removed corresponds to 15 and 18 MeV exclusions for the $E/A = 20$ and 35 MeV cases, respectively. Subtraction of these values from the center of mass energies gives 220 and 391 MeV for the two cases. The Q values were calculated for the reactions $^{14}\mathrm{N} + {}^{107}\mathrm{Ag} \rightarrow {}^{7}\mathrm{Li} + {}^{114}\mathrm{Sb}$ and $^{14}\mathrm{N} + {}^{109}\mathrm{Ag} \rightarrow {}^{7}\mathrm{Li} + {}^{116}\mathrm{Sb}$ and the average value of -15 MeV was used. This gave 206 and 376 MeV as the lower limits for the excitation energies for the two beam energies.

For convenience, the HMB model is compared to the moving source model, rather than the data. Since the HMB model is a phase space calculation, it predicts only the neutron energy distribution, (dM/dE), whereas Eq. (7) gives ($d^2M/dE\,d\Omega$) in terms of the moving source fit parameters. However, integration of that equation over solid angle, $d\Omega$, gives[43]

$$\frac{dM}{dE} = \frac{M_i}{\sqrt{(\pi \epsilon_i k T_i)}} \exp[-(E + \epsilon_i)/kT_i] \times \sinh[2\sqrt{(\epsilon_i E)}/kT_i] \,, \tag{15}$$

where the sum over $i = 1,2$ is implied. Generally, the agreement between the moving source model and the data is excellent, so a comparison of the two models is nearly equivalent to comparing the HMB model to the data.

The HMB model does not include any dependence on the IMF with which the neutrons are in coincidence. However, since the neutron moving source fit parameters do not depend strongly on the coincident isotope (based on the results shown in Tables III and IV) neutrons associated with a specific fragment will be compared directly to the HMB model predictions. (^{7}Li is chosen as it has the best statistics.) Putting the fit parameters from Table III (including the errors on the parameters) for neutrons

in coincidence with ^{7}Li (where the multiplicities used are the linear average of the in-plane and out-of-plane values) into Eq. (15) for discrete neutron energies gives the representative points shown in Figs. 8 and 9 (for $E/A=20$ and 35 MeV, respectively).

As stated earlier, the most naive approach suggests that $n_0=A_p$, while a first change from that might be $n_0=A_p+3$. Calculations based on these two choices are shown in Fig. 8 (with both $E^*=206$ and 246 MeV for $E/A=20$ MeV) and Fig. 9 (with both $E^*=376$ and 432 MeV for $E/A=35$ MeV). It is important to note that while the normalization of the moving source model is a parameter fit to the data, the normalization of the HMB model is absolute. In both of these figures, the HMB model predictions are shown for three time slices in the reaction: $t=0.2$, 2.0, and 4.0×10^{-21} s after the collision. Generally, the best agreement between the two models (and, hence, between the HMB model and the data) occurs for $n_0=A_p(=14)$ and for the lower limit of the excitation energy (i.e., excluding the energy associated with the IMF emission). However, the higher exciton number along with the higher excitation energy gives similar agreement. While the data does not eliminate either of these possibilities, it certainly seems to support the limits established. The HMB model is able to describe all of the data presented here with reasonable limits on the parameters.

These results contrast somewhat to those presented in Refs. 42, 49, and 64. In their paper on light particle emission from ^{16}O+^{197}Au reactions at 140, 215, and 310 MeV, Awes *et al.* report that to describe the proton spectra, exciton numbers of 18, 25, and 30 must be assumed for the three beam energies, respectively.[64] In addition, in both Refs. 42 and 49, agreement between the HMB model and the neutron data could be obtained only with arbitrary normalizations. In addition, Holub *et al.* summarize what is described as an energy dependence of n_0. The dependence is given as a function of $(E_{\text{c.m.}}-V_C)/\mu$, where $E_{\text{c.m.}}$ is the center of mass energy, V_C is the Coulomb barrier, and μ is the reduced mass. For the present work, this value is 16 and 31 MeV/nucleon for $E/A=20$ and 35 MeV, respectively. The results presented in this paper do not contradict the statement in Ref. 49 that for $(E_{\text{c.m.}}-V_C)/\mu>20$ MeV/nucleon, n_0 is constant at roughly A_p+3. However, based on the $E/A=20$ MeV data where $(E_{\text{c.m.}}-V_C)/\mu=16$, the present work does not support the observation of a pronounced rise in n_0 above A_p+3 for $5<(E_{\text{c.m.}}-V_C)/\mu<20$ MeV/nucleon. In the present work, no evidence is seen which would necessitate an energy dependence of n_0, and there is no evidence that n_0 is greater than A_p+3. In both that respect and the overall normalization of the HMB predictions, the HMB model appears to agree with the data very well.

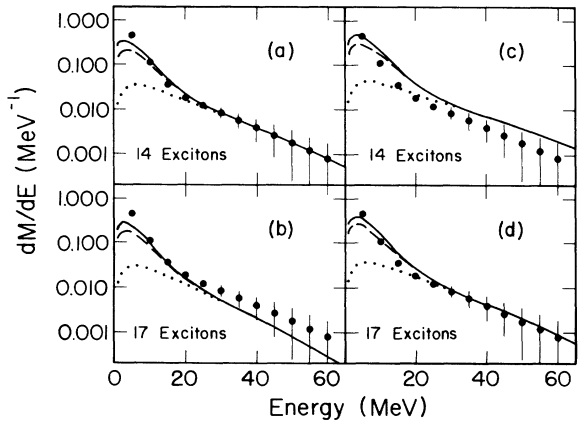

FIG. 8. Neutron energy distribution from moving source model (representative points plotted) for $E/A=20$ MeV compared to that from HMB model (lines) for 206 MeV excitation energy [(a) and (b)] and 246 MeV excitation energy [(c) and (d)]. In each case the dotted lines are at $t=0.2\times10^{-21}$ s, the dashed lines at $t=2.0\times10^{-21}$ s, and the solid lines at $t=4.0\times10^{-21}$ s.

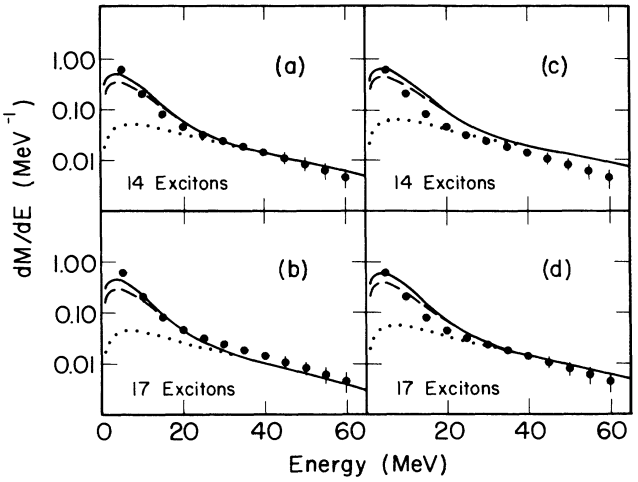

FIG. 9. Neutron energy distribution from moving source model (representative points plotted) for $E/A=35$ MeV compared to that from HMB model (lines) for 376 MeV excitation energy [(a) and (b)] and 432 MeV excitation energy [(c) and (d)]. In each case the dotted lines are at $t=0.2\times10^{-21}$ s, the dashed lines at $t=2.0\times10^{-21}$ s, and the solid lines at $t=4.0\times10^{-21}$ s.

Finally, the HMB model predicts the time evolution of the system. The predictions given by this model are entirely consistent with the two-source moving source model and more quantitative. From Figs. 8 and 9, it can be seen that the PE component of the evaporation occurs entirely within the first 0.2×10^{-21} s. On the other hand, it takes 10–20 times as long for the target residue to reach equilibrium. This reinforces the moving source model description of the PE neutron emission being very prompt, and the target residue emission being of a compound nucleus like sequential nature (hence, it occurs over a much longer time span).

V. SUMMARY AND CONCLUSIONS

A. Summary

Kinetic energy spectra were obtained for neutrons in coincidence with intermediate mass fragments observed

at 50°, 70°, and 90° in the lab from the reaction of $^{14}N+Ag$ at both $E/A=20$ and 35 MeV. While there have been numerous previous neutron coincidence experiments,[40–51] these were limited to measuring neutrons in coincidence with either projectile-like fragments, fission fragments, or evaporation residues. The present measurement represents the first time that neutrons have been measured in coincidence with intermediate-mass fragments observed at large angles.

These neutron kinetic energy spectra were fitted with a two-source moving source model.[11] This model provided an excellent parametrization of the data in terms of an associated multiplicity, an effective temperature parameter, and a source velocity for both a target like source and a preequilibrium source. The associated neutron multiplicities for neutrons in coincidence with ^{6}Li, ^{7}Li, ^{8}Li, ^{7}Be, ^{9}Be, ^{10}Be, ^{10}B, and ^{11}B fragments are reported in Tables III and IV. For $E/A=20$ MeV, the target-like source multiplicity is typically 4–5 (depending primarily on the type of fragment with which the neutrons were in coincidence) while the PE source multiplicity is about 1. For the $E/A=35$ MeV data these values are 6–7 and 2, respectively. No dependence is seen on fragment angle over the angular range investigated here. No preference is seen for the neutrons to be emitted either on the same side or on the opposite side of the beam as the observed fragment. An out-of-plane anisotropy is observed. It is approximately 20% for the target residue source and about 50% for the PE source. The measured multiplicities are used to replace estimates used by Boal[33] to determine the effect of final state interactions on bound excited state population measurements. While the observed multiplicities are significantly different from those estimates, the model is fairly insensitive to these values in this region, and the correction to its effects are negligible.

A physically significant interpretation of the source velocities and effective temperature parameters can be made. For the target residue source, the velocities are 80 and 65% of the center of mass velocity for $E/A=20$ and 35 MeV, respectively. Typical corresponding effective temperature parameters (from the fits) are 2.5 and 3 MeV. These values are reasonably close to what would be expected for incomplete fusion. For the PE source, the velocities are approximately 35% of the beam velocity for both beam energies. The corresponding effective temperature parameters are approximately 10 and 12 MeV. These values are similar to values obtained for particle inclusive measurements of fragments from $Z=1$ to $Z=7$.

Finally, by integrating the moving source model's analytic expression for the neutron spectra over solid angle an expression for the neutron energy distribution (dM/dE), is obtained. With the above moving source fit parameters, this energy distribution is then readily compared to predictions made by the Boltzmann master equation approach of Harp, Miller, and Berne as modified for heavy ion induced reactions by Blann.[20] Reasonable agreement is obtained for exciton number, n_0, equal to either the number of beam nucleons, A_p, or for $n_0=A_p+3$. The agreement is both in the shape of the energy distribution (i.e., its energy dependence) and in the overall normalization (i.e., associated multiplicity). This is contrast to several similar works.[42,49,64,66]

B. Conclusions

An important component of heavy ion reaction studies in this energy region (10 MeV $\leq E/A \leq 100$ MeV) has been the observation of intermediate mass fragments ($4 < A < A_p$) at large angles ($\theta \gg \theta_{grazing}$).[16,34–37] Since this is the first measurement of neutrons in coincidence with fragments of this type, many interesting conclusions can be drawn.

A logical comparison to make is between the results presented here and those from neutrons in coincidence with IMF's at forward angles (projectile-like fragments). In Ref. 50, a definite increase in the observed target residue associated neutron multiplicities is seen as a function of IMF angle. That trend contrasts with the data presented here, in which no significant dependence on fragment angle is observed. The events associated with fragments observed at any given angle reflect a range of impact parameters. As the observed fragment angle is increased, the range of impact parameters is biased towards more violent collisions, up to a maximum angle. After that point, it appears the collisions are all characterized by fairly central collisions (giving rise to the highest average associated multiplicities). Generally, the observed multiplicities are also consistent with those seen from neutrons in coincidence with evaporation residues for similar reactions.[42,49]

The moving source model is generally successful at describing the energy spectra of fragments emitted from such reactions. The present neutron data are no exception, with excellent fits to the in-plane data provided by a two source description. However, the assumption of isotropic emission (in the moving source frame) in that model is in conflict with the observed data which show an out-of-plane anisotropy. For that reason, caution should be used when interpreting the source parameters (particularly the source velocity and the effective temperature parameter). As shown by Chitwood *et al.*, the observed parameters can vary significantly if similar models with different assumptions are adopted.[39] For this particular case, a preferred plane of emission is probably due the angular momentum of the system. Typically, the observed IMF had less than 20% of the beam momentum. This restricts the determination of the reaction plane, with the implication that the observed anisotropy is a lower limit. It is likely that the coincident fragments did not provide the most effective determination of the reaction plane.

One application of the associated neutron multiplicities is in the calculation of the effects of final state interactions on bound excited state population measurements. Boal made such a calculation using a relatively simple model[33] and estimated associated fragment multiplicities. The measurement of these associated PE neutron multiplicities combined with measurements of the associated PE multiplicities for light charge particles for similar reactions[37] allowed Boal's calculation to be redone with more accurate estimates of the necessary parameters.

The model is very insensitive to the multiplicities in this region, however, and the results are little changed. Basically, Boal was able to conclude that final state interactions could lower the observed temperatures by an order of magnitude from the emission temperature. Based on the model he used, this result remains. However, as pointed out in Ref. 28, that model of cooling is one limiting case. In their paper, Morrissey *et al.* also present a model at the opposite limit (predicting the minimum cooling instead of the maximum). Now that reasonable estimates of the associated multiplicities are available a more sophisticated model would be very useful.

For this data, the HMB model also provided a good description. Essentially, this model makes several assumptions about the physics of the problem, and then makes predictions without any adjustable parameters. If the predictions match the data well, one would hope to be able to conclude that the physical approximations are fairly reasonable. However, recently attempted applications of the basic model have been somewhat unsuccessful.[42,49,64,66] In order to explore the possibilities, adjustments in the parameters have been introduced.[42,49,64] These include letting the exciton number be a free parameter, generally energy dependent, adjusting the intranuclear transition rates, and including arbitrary overall normalizations to the cross section. While these may aid in the description of the data, it is not clear that any conclusions can then be made with regards to the physics. Finally, it is possible that such adjustments may not be necessary. It may be that agreement with the data is actually being accomplished with offsetting adjustments. This is suggested by Blann[24] as the explanation for the result obtained by Holub *et al.*[42] In particular, large values of n_0 can be offset by arbitrary normalizations of the cross section combined with different intranuclear transition rates. However, such a cancellation of errors is more easily obtained when observing only the PE contribution to the neutron spectrum. By including the neutrons from both sources, the problem becomes more constrained. The agreement obtained here with the HMB model is both for the total spectrum shape and the multiplicity. Furthermore, the model predicts the time development of the neutron spectrum.

ACKNOWLEDGMENTS

We would like to thank G. Caskey for his valuable help. We would also like to extend our appreciation to M. Blann for making his HMB code available to us. C. Bloch would like to acknowledge the support of Indiana University Cyclotron Facility during the preparation of this paper. Finally, we would like to thank the staff of the National Superconducting Cyclotron Laboratory for making this experiment possible. This work was supported by the National Science Foundation under Grant Nos. PHY-83-12245 and PHY-86-11210.

*Present address: Indiana University Cyclotron Facility, 2401 Milo B. Sampson Lane, Bloomington, IN 47401.

†Present address: Hughes Aircraft, El Segundo, CA 90245.

‡Present address: School of Physics and Astronomy, Univeristy of Minnesota, Minneapolis, MN 55455.

§Present address: Lawrence Livermore National Laboratory, Livermore, CA 94550.

**On leave at Kernchemie, Gesellschaft für Schwerionenforschung, 1 Planck Strasse, D-6100 Darmstadt 11, Federal Republic of Germany.

[1]G. D. Westfall, J. Gosset, P. J. Johansen, A. M. Poskanzer, W. G. Meyer, H. H. Gutbrod, A. Sandoval, and R. Stock, Phys. Rev. Lett. **37**, 1202 (1976).

[2]F. Pühlhofer, Nucl. Phys. **A280**, 267 (1977).

[3]J. Cugnon, Phys. Rev. C **22**, 1885 (1980).

[4]J. Negele, Rev. Mod. Phys. **54**, 913 (1982).

[5]D. J. Morrissey, C. Bloch, W. Benenson, E. Kashy, R. A. Blue, R. M. Ronningen, and R. Aryaeineyad, Phys. Rev. C **34**, 761 (1986).

[6]B. V. Jacak, G. D. Westfall, G. M. Crawley, D. Fox, C. K. Gelbke, L. H. Harwood, B. E. Hasselquist, W. G. Lynch, D. K. Scott, H. Stöcker, M. B. Tsang, G. Buchwald, and T. J. M. Symons, Phys. Rev. C **35**, 1751 (1987).

[7]G. Bertsch and P. J. Siemens, Phys. Lett. **126B**, 9 (1983).

[8]M. W. Curtin, H. Toki, and D. K. Scott, Phys. Lett. **123B**, 289 (1983).

[9]D. Boal, Phys. Rev. C **30**, 119 (1984).

[10]C. B. Chitwood, D. J. Fields, C. K. Gelbke, W. G. Lynch, A. D. Panagiotou, M. B. Tsang, H. Utsunomiya, and W. A. Friedman, Phys. Lett. **131B**, 289 (1983).

[11]B. V. Jacak, G. D. Westfall, C. K. Gelbke, L. H. Harwood, W. G. Lynch, D. K. Scott, H. Stöcker, M. B. Tsang, and T. J. M. Symons, Phys. Rev. Lett. **51**, 1846 (1983).

[12]W. G. Lynch, C. B. Chitwood, M. B. Tsang, D. J. Fields, D. R. Klesch, C. K. Gelbke, G. R. Young, T. C. Awes, R. L. Ferguson, F. E. Obenshain, F. Plasil, R. L. Robinson, and A. D. Panagiotou, Phys. Rev. Lett. **51**, 1850 (1983).

[13]D. J. Fields, W. G. Lynch, C. B. Chitwood, C. K. Gelbke, M. B. Tsang, H. Utsunomiya, and J. Aichelin, Phys. Rev. C **30**, 1912 (1984).

[14]A. S. Hirsch, A. Bujak, J. E. Finn, L. J. Gutay, R. W. Minich, N. T. Porile, R. P. Scharenberg, B. C. Stringfellow, and F. Turkot, Phys. Rev. C **29**, 508 (1984).

[15]D. J. Morrissey, W. Benenson, E. Kashy, B. Sherrill, A. D. Panagiotou, R. A. Blue, R. M. Ronningen, J. van der Plicht, and H. Utsunomiya, Phys. Lett. **148B**, 423 (1984).

[16]G. D. Westfall, Z. M. Koenig, B. V. Jacak, L. H. Harwood, G. M. Crawley, M. W. Curtin, C. K. Gelbke, B. Hasselquist, W. G. Lynch, A. D. Panagiotou, D. K. Scott, H. Stöcker, and M. B. Tsang, Phys. Rev. C **29**, 861 (1984).

[17]J. Pochodzalla, W. A. Firedman, C. K. Gelbke, W. G. Lynch, M. Maier, D. Ardouin, H. Delagrange, H. Doubre, C. Grégoire, A. Kyanowski, W. Mittig, A. Péghaire, J. Péter, F. Saint-Laurent, Y. P. Viyogi, B. Zwieglinski, G. Bizard, F. Lefebures, B. Tamain, and J. Québert, Phys. Rev. Lett. **55**, 177 (1985); Phys. Lett. **161B**, 275 (1985).

[18]L. G. Sobotka, D. G. Sarantites, H. Puchta, F. A. Dilmanian, and M. Jääskeläinen, M. L. Halbert, J. H. Barker, J. R. Beene, R. L. Ferguson, D. C. Hensley, and G. R. Young, Phys. Rev. C **34**, 917 (1986).

[19]R. Wada, K. D. Hildenbrand, U. Lynen, W. F. J. Müller, H. J. Rabe, H. Sann, H. Stelzer, W. Trautmann, R. Trockel, N. Brummund, R. Glasow, K. H. Kampert, S. Santo, E. Eckert, J. Pochodzalla, I. Bock, and D. Pelte, Phys. Rev. Lett. **58**, 1829 (1987).

[20]M. Blann, Phys. Rev. C **23**, 205 (1981).

[21]G. Fái and J. Randrup, Nucl. Phys. **A381**, 557 (1982).

[22]W. A. Friedman and W. G. Lynch, Phys. Rev. C **28**, 950 (1983).

[23]A. D. Panagiotou, M. W. Curtin, H. Toki, D. K. Scott, and P. J. Siemens, Phys. Rev. Lett. **52**, 496 (1984).

[24]M. Blann, Phys. Rev. C **31**, 1245 (1985).

[25]A. D. Panagiotou, M. W. Curtin, and D. K. Scott, Phys. Rev. C **31**, 55 (1985).

[26]D. Hahn and H. Stöcker, Nucl. Phys. **A476**, 718 (1988); Phys. Rev. C **35**, 1311 (1987).

[27]M. E. Fisher, Physics (N.Y.) **3**, 355 (1967).

[28]D. J. Morrissey, W. Benenson, E. Kashy, C. Bloch, M. Lowe, R. A. Blue, R. M. Ronningen, B. Sherrill, H. Utsunomiya, and I. Kelson, Phys. Rev. C **32**, 877 (1985).

[29]C. Bloch, W. Benenson, E. Kashy, D. J. Morrissey, R. A. Blue, R. M. Ronningen, and H. Utsunomiya, Phys. Rev. C **34**, 850 (1986).

[30]G. D. Doolen, Phys. Rev. Lett. **40**, 1695 (1978).

[31]C. Bloch, W. Benenson, A. I. Galonsky, E. Kashy, J. Heltsley, L. Heilbronn, M. Lowe, B. Remington, D. J. Morrissey, and J. Kasagi, Phys. Rev. C **36**, 203 (1987).

[32]C. B. Chitwood, C. K. Gelbke, J. Pochodzalla, Z. Chen, D. J. Fields, W. G. Lynch, R. Morse, M. B. Tsang, D. H. Boal, and J. C. Shillcock, Phys. Lett. B **172**, 27 (1986).

[33]D. Boal, Phys. Rev. C **30**, 749 (1984).

[34]W. G. Meyer, H. H. Gutbrod, C. Lukner, and A. Sandoval, Phys. Rev. C **22**, 179 (1980).

[35]G. D. Westfall, B. V. Jacak, N. Anantaraman, M. W. Curtin, G. M. Crawley, C. K. Gelbke, B. Hasselquist, W. G. Lynch, D. K. Scott, M. B. Tsang, M. J. Murphy, T. J. M. Symons, R. Legrain, and T. J. Majors, Phys. Lett. **116B**, 118 (1982).

[36]K. L. Wolf, J. P. Sullivan, G. M. Berkowitz, H. L. Kent, K. M. Pierpoline, B. S. Potts, C. T. Spillett, and J. Schoemaker, Intermediate Mass Fragment Emission, contribution to the Symposium on Nuclear Physics at Oaxtepec, Mexico, 1985.

[37]D. J. Fields, W. G. Lynch, T. K. Nayak, M. B. Tsang, C. B. Chitwood, C. K. Gelbke, R. Morse, J. Wilczyński, T. C. Awes, R. L. Ferguson, F. Plasil, F. E. Obenshain, and G. R. Young, Phys. Rev. C **34**, 536 (1986).

[38]A. M. Poskanzer, G. W. Butler, E. K. Hyde, Phys. Rev. **3**, 882 (1971).

[39]C. B. Chitwood, D. J. Fields, C. K. Gelbke, D. R. Klesch, W. G. Lynch, M. B. Tsang, T. C. Awest, R. L. Ferguson, F. E. Obenshain, F. Plasil, R. L. Robinson, and G. R. Young, Phys. Rev. C **34**, 858 (1986).

[40]D. Hilscher, J. R. Birkelund, A. D. Hoover, W. U. Schröder, W. W. Wilke, J. R. Huizenga, A. C. Mignerey, K. L. Wolf, H. F. Breuer, and V. E. Viola, Jr., Phys. Rev. C **20**, 576 (1979).

[41]A. Gavron, J. R. Beene, B. Cheynis, R. L. Ferguson, F. E. Obenshain, F. Plasil, G. R. Young, G. A. Petitt, C. F. Maguire, D. G. Sarantites, M. Jääskeläinen, and K. Geoffroy-Young, Phys. Rev. C **27**, 450 (1983).

[42]E. Holub, D. Hilscher, G. Ingold, U. Jahnke, H. Orf, and H. Rossner, Phys. Rev. C **28**, 252 (1983).

[43]E. Holub, M. Korolija, and N. Cindor, Z. Phys. A **314**, 347 (1983).

[44]D. Hilscher, E. Holub, G. Ingold, U. Jahnke, H. Orf, H. Rossner, W. P. Zank, W. U. Schröder, H. Gemmeke, K. Keller, L. Lassen, and W. Lücking, in *Proceedings of the Workshop on Coincidence Particle Emission from Continuum States in Nuclei, Bad Honnef, 1984,* edited by H. Machner and P. Jahn (World-Scientific, Singapore, 1984), p. 268.

[45]G. Caskey, A. Galonsky, B. Remington, M. B. Tsang, C. K. Gelbke, A. Kiss, F. Deák, Z. Seres, J. J. Kolata, J. Hinnefeld, and J. Kasagi, Phys. Rev. C **31**, 1597 (1985).

[46]G. Caskey, A. Galonsky, B. Remington, F. Deák, A. Kiss, and Z. Seres, Phys. Rev. C **34**, 506 (1986).

[47]F. Deák, A. Kiss, Z. Seres, G. Caskey, A. Galonsky, B. Remington, C. K. Gelbke, M. B. Tsang, and J. J. Kolata, Nucl. Phys. **A464**, 133 (1987).

[48]F. Deák, A. Kiss, Z. Seres, G. Caskey, A. Galonsky, and B. Remington, Nucl. Instrum. Methods Phys. Res. **A258**, 67 (1987).

[49]E. Holub, D. Hilscher, G. Ingold, U. Jahnke, H. Orf, H. Rossner, W. P. Zank, W. U. Schröder, H. Gemmeke, K. Keller, L. Lassen, and W. Lücking, Phys. Rev. C **33**, 143 (1986).

[50]B. A. Remington, G. Caskey, A. Galonsky, C. K. Gelbke, L. Heilbronn, J. Heltsley, M. B. Tsang, F. Deák, A. Kiss, Z. Seres, J. Kasagi, and J. J. Kolata, Phys. Rev. C **34**, 1685 (1986); B. A. Remington, Ph.D. thesis, Michigan State University, 1986.

[51]D. Hilscher, H. Rossner, A. Gamp, U. Jahnke, B. Cheynis, B. Chambon, D. Drain, C. Pastor, A. Giorni, C. Morand, A. Dauchy, P. Stassi, and G. Petitt, Phys. Rev. C **36**, 208 (1987).

[52]A. Vander Molen, R. Au, R. Fox, and T. Glynn, Nucl. Instrum. Methods **A236**, 359 (1985).

[53]J. F. Ziegler, *Handbook of Stopping Cross-sections* (Pergamon, New York, 1980).

[54]R. J. Kurtz, University of California Radiation Lab Internal Report No. UCRl-11339, 1964.

[55]R. A. Cecil, B. D. Anderson, and R. Madey, Nucl. Instrum. Methods **161**, 439 (1979).

[56]G. D. Westfall, R. G. Sextro, A. M. Poskanzer, A. M. Zebelman, G. W. Butler, and E. K. Hyde, Phys. Rev. C **17**, 1368 (1978).

[57]J. H. Heltsley, L. Brandon, A. Galonsky, L. Heilbronn, B. A. Remington, S. Langer, A. Vander Molen, and J. Yurkon, Nucl. Instrum. Methods **A263**, 441 (1988).

[58]A. S. Goldhaber, Phys. Rev. C **17**, 2243 (1978).

[59]K. J. Le Couteur and D. W. Lang, Nucl. Phys. **13**, 32 (1959).

[60]A. Kiss, F. Deák, Z. Seres, G. Caskey, A. Galonsky, L. Heilbronn, B. A. Remington, and J. Kasagi, Phys. Lett. B **184**, 149 (1987).

[61]T. C. Awes, C. K. Gelbke, G. Poggi, B. B. Back, B. Glagola, H. Breuer, V. E. Viola, Jr., and T. J. M. Symons, Phys. Rev. Lett. **45**, 513 (1980).

[62]T. C. Awes, G. Poggi, C. K. Gelbke, B. B. Back, B. G. Glagola, H. Breuer, and V. E. Viola, Jr., Phys. Rev. C **24**, 89 (1981).

[63]T. C. Awes, G. Poggi, S. Saini, C. K. Gelbke, R. Legrain, and G. D. Westfall, Phys. Lett. **103B**, 417 (1981).

[64]T. C. Awes, S. Saini, G. Poggi, C. K. Gelbke, D. Cha, R. Legain, and G. D. Westfall, Phys. Rev. C **25**, 2361 (1982).

[65]C. Bloch and E. Kashy, Phys. Rev. C **36**, 855 (1987).

[66]A. Gavron, J. R. Beene, R. L. Ferguson, F. E. Obenshain, F. Plasil, G. R. Young, G. A. Petitt, K. Geoffroy Young, M. Jääskeläinen, D. G. Sarantites, and C. F. Maguire, Phys. Rev.

C **24**, 2048 (1981).
[67]C. K. Gelbke, M. Bini, C. Olmer, D. L. Hendrie, J. L. Laville, J. Mahoney, M. C. Mermaz, D. K. Scott, and H. H. Wieman, Phys. Lett. **71B**, 83 (1977).
[68]D. H. E. Gross and J. Wilczyński, Phys. Lett. **67B**, 1 (1977).
[69]R. Weiner and M. Weström, Nucl. Phys. **A286**, 282 (1977).
[70]J. P. Bondorf, J. N. De, G. Fái, A. O. Karvinen, B. Jakobsson, and J. Randrup, Nucl. Phys. **A333**, 285 (1980).
[71]T. Ericson and V. Strutinski, Nucl. Phys. **8**, 284 (1958).
[72]Louis C. Vaz and John M. Alexander, Phys. Rep. **97**, 1 (1983).
[73]M. B. Tsang, C. B. Chitwood, D. J. Fields, C. K. Gelblke, D. R. Klesch, W. G. Lynch, K. Kwiatkowski, and V. E. Viola, Jr., Phys. Rev. Lett. **52**, 1967 (1984).
[74]W. P. Zank, D. Hilscher, G. Ingold, U. Jahnke, M. Lehmann, and H. Rossner, Phys. Rev. C **33**, 519 (1986).
[75]J. Péter, M. Berlanger, C. Ngô, B. Tamain, B. Lucas, C. Mazur, M. Ribrag, and C. Signarbieux, Z. Phys. A **283**, 413 (1977).
[76]Y. Eyal, A. Gavron, I. Tserruya, Z. Fraenkel, Y. Eisen, S. Wald, R. Bass, G. R. Gould, G. Kreyling, R. Renfordt, K. Stelzer, R. Zitzmann, A. Gobbi, U. Lynen, H. Stelzer, I. Rode, and R. Bock, Phys. Rev. Lett. **41**, 625 (1978).
[77]K. A. Geoffroy, D. G. Sarantites, L. Westerberg, J. H. Barker, D. C. Hensley, R. A. Dayras, and M. L. Halbert, Bull. Am. Phys. Soc. **23**, 950 (1978).
[78]D. L. Hillis, O. Christensen, B. Fernandez, A. J. Ferguson, J. D. Garrett, G. B. Hagemann, B. Herskind, B. B. Back, and F. Folkmann, Phys. Lett. **78B**, 405 (1978).
[79]L. Westerberg, D. G. Sarantites, D. C. Hensely, R. A. Dayras, M. L. Halbert, and J. H. Barker, Phys. Rev. C **18**, 796 (1978).
[80]V. E. Viola, Jr., B. B. Back, K. L. Wolf, T. C. Awes, C. K. Gelbke, and H. Breuer, Phys. Rev. C **26**, 178 (1982).
[81]G. la Rana, G. Nebbia, E. Tomasi, C. Ngô, X. S. Chen, S. Leray, P. Lhenoret, R. Lucas, C. Mazur, M. Ribrag, C. Cerruti, S. Chiodelli, A. Demeyer, D. Guinet, J. L. Charvet, M. Morjean, A. Péghaire, Y. Pranal, L. Sinopoli, J. Uzureau, and R. de Swiniarski, Nucl. Phys. **A407**, 233 (1983).
[82]J. Jastrzebski, P. P. Singh, T. Mróz, S. E. Vigdor, M. Fatyga, and H. J. Karwowski, Phys. Rev. C **34**, 60 (1986).